Experimental Study of Residual Stresses in Laser Clad AISI P20 Tool Steel on Pre-Hardened Wrought P20 Substrate

Chen, J.-Y.; Conlon, K.; Xue, L.; Rogge, R.

Publisher's version / Version de l'éditeur:
https://doi.org/10.1016/j.msea.2010.07.098
Materials Science and Engineering A, 527, 27/28, pp. 7265-7273, 2010-07-01

Materials Science and Engineering A 527 (2010) 7265–7273

Contents lists available at ScienceDirect

Materials Science and Engineering A

journal homepage: www.elsevier.com/locate/msea

Experimental study of residual stresses in laser clad AISI P20 tool steel on pre-hardened wrought P20 substrate

J.-Y. Chen [a,*], K. Conlon [b], L. Xue [a], R. Rogge [b]

[a] Industrial Materials Institute, National Research Council of Canada, 800 Collip Circle, London, Ontario, Canada N6G 4X8
[b] Steacie Institute for Molecular Sciences, National Research Council of Canada, Chalk River Laboratories, Stn.18, Chalk River, Ontario, Canada K0J 1J0

ARTICLE INFO

Article history:
Received 7 February 2010
Received in revised form 11 July 2010
Accepted 29 July 2010

Keywords:
Laser cladding
AISI P20 tool steel
Residual stress
Neutron diffraction
Hole-drilling method
Tooling repair

ABSTRACT

Laser cladding is to deposit desired material onto the surface of a base material (or substrate) with a relatively low heat input to form a metallurgically sound and dense clad. This process has been successfully applied for repairing damaged high-value tooling to reduce their through-life cost. However, laser cladding, which needs to melt a small amount of a substrate along with cladding material, inevitably introduces residual stresses in both clad and substrate. The tensile residual stresses in the clad could adversely affect mechanical performance of the substrate being deposited. This paper presents an experimental study on process-induced residual stresses in laser clad AISI P20 tool steel onto pre-hardened wrought P20 base material and the correlation with microstructures using hole-drilling and neutron diffraction methods. Combined with X-ray diffraction and scanning electron microscopic analyses, the roles of solid-state phase transformations in the clad and heat-affected zone (HAZ) of the substrate during cladding and post-cladding heat treatments on the development and controllability of residual stresses in the P20 clad have been investigated, and the results could be beneficial to more effective repair of damaged plastic injection molds made by P20 tool steel.

1. Introduction

Laser cladding by blown powder or wire feeding can deposit a layer of material onto the surface of a similar or dissimilar base material (or substrate) to produce a metallurgically sound and dense clad. In the last 20 years, many relevant applications have been reported [1–3], the majority of which, can be divided into two areas: (1) laser cladding to deposit high-performance material on high-value component or tooling made by different base material to enhance its local (or entire) surface properties, such as the resistance against corrosion, wear, or high-temperature oxidation, etc.; the component or tooling made by the above hybrid materials can provide an overall mechanical performance which no single material can provide and in addition, they often can save overall costs of raw materials and manufacturing process by allowing optimal material to be used in needed location(s), and (2) laser cladding (or laser cladding base free-form fabrication) to repair or restore original geometries and functionalities of a worn or damaged high-value component or tooling and sometimes, to restore undersized expensive material due to machining or grinding errors. It is no doubt that other alternative processes are also available for the similar applications such as TIG welding, thermal spraying, gas dynamic spraying (GDS), e-beam deposition and others. Considering various factors relevant to the costs of materials, equipment and manufacturing processes, and the quality of deposited materials, laser cladding has demonstrated some unique advantages over others: it can produce metallurgically sound and dense clad layer using a relatively low heat input which minimizes the distortion of the component or tooling being deposited; it produces metallurgical bond between the clad layer and the substrate; and it can control the dilution of cladding material into the substrate to reduce undesired deterioration of mechanical properties of the base material. The National Research Council's Industrial Materials Institute (NRC-IMI-London) has been developing laser cladding base processes for more than a decade, targeting at automotive, aerospace and other manufacturing industrial applications [4–8].

The objective of present research aims at laser cladding to deposit AISI P20 tool steel onto pre-hardened wrought AISI P20 substrate for the purpose of repairing and restoring damaged tooling. The P20, a kind of low carbon tool steel containing chromium and molybdenum alloying elements, is commonly used for making plastic injection molds. The P20 tool steel is thermally hardenable through proper heat treatments [9], providing a reasonably good wear and corrosion resistances. The plastic injection molds made by P20 tool steel, however, still frequently require some forms of repair by welding [10] because of the damages/worn-out in the molds, the errors in machining or the changes in design required during manufacturing. Laser cladding has been identified as a promising

* Corresponding author. Tel.: +1 519 430 7067; fax: +1 519 430 7064.
E-mail address: jianyin.chen@nrc.gc.ca (J.-Y. Chen).

0921-5093/$ – see front matter.
doi:10.1016/j.msea.2010.07.098

process for repairing and restoring original dimensions and functionalities of those molds to extend their service life and in addition, for enhancing or re-configuring existing molds for their subsequent re-use, to substantially reduce their through-life costs [11].

Nevertheless, it should be realized that laser cladding of tool steels, in spite of relatively low heat input, still need melt a small portion of base material (or substrate) along with cladding material, which would introduce certain amount of residual stresses in both clad and substrate. It is well known that residual stresses, defined as intrinsic self-equilibrating stresses, exist without external forces. They arise as consequences of various thermal treatments, which cause thermal gradients and phase transformations, as well as of thermo-mechanical processing, which causes local elastic or plastic deformation [12]. For laser cladding process, in general, the major causes of process-induced residual stresses in a clad layer are ascribed to two effects [11,13–15]: (1) thermal mismatch among the clad, the heat-affected zone (HAZ) and the unaffected cold substrate when a clad cools after it re-solidifies, and/or (2) solid-state-phase-transformation induced volumetric change in the clad and the underneath HAZ of the substrate when the clad cools after it re-solidifies. In most cases, tensile residual stresses may arise in the clad, which cause potential cracking within the clad and/or the substrate, and adversely affect ultimate mechanical performance (such as fatigue strength or resistance to stress corrosion) and dimensional stability (i.e., distortion) of the base material being deposited. Even so, it could still be expected that this problem could be lessened or resolved by various approaches, such as optimizing processing parameters, creating an interlayer to minimize the thermal mismatch between the clad and the substrate, preheating the substrate during cladding, or performing post-cladding stress-relieving treatments, etc. [16,17].

To have a comprehensive understanding on the nature of residual stresses in the clad and their controllability will be beneficial to the development of laser cladding process and the improvement of in-service mechanical performance of the base material being deposited (here it is referred to the plastic injection molds made by P20 tool steel). The residual stresses, however, could not be measured directly, but only deduced from the measured strains by using elastic constants. Moreover, to quantify these stresses within a clad layer is not always straightforward. Generally, numerical simulation and modeling are popular approaches in predicting residual stresses in the clad layer [18–20], but those predictions require comprehensive knowledge of thermo-physical and thermo-mechanical properties of the materials and their evolution as a function of temperature, which are not always available to the investigators. Moreover, extensive experiments are still required to validate those theoretical predictions. Nevertheless, experimental studies of process-induced residual stresses are still the most adopted approaches in laser cladding [21–26]. Existing measurement techniques can be divided into mechanical stress relaxation methods (such as hole-drilling) and nondestructive methods (such as X-ray and neutron diffraction), which are based on the relationship between physical or crystallographic parameters and residual stresses [27]. The hole-drilling method can be used to determine average stress level in a clad layer, which measures relieved strains by the frozen residual stresses surrounding a hole being drilled on the surface of the clad, but the sensitivity of the measurement rapidly declines with increasing the depth of the hole. X-ray and neutron diffraction methods are based on the measurement of lattice strains by studying the variations in crystal lattice parameters of a polycrystalline material: the first method measures the residual strain on the near-surface of the material; and the second one measures the residual strain within a volume of the sample. Since X-ray diffraction technique is limited to sample the near-surface information, and mechanical/electrochemical layer removal is required to obtain the through-thickness information on the clad and substrate. By contrast, neutron diffraction can nondestructively obtain profiles of residual stresses across the clad and substrate. However, this method requires a special neutron source. Both hole-drilling and neutron diffraction have the capability to measure the residual stresses in a clad with the existence of certain degree of directionally solidified microstructure induced by laser cladding [28], while this type of preferred crystallographic orientation in the clad indeed arises some concerns during X-ray diffraction measurement using conventional $\sin^2\Psi$ method [29]. It is understood that an appropriate choice of adequate techniques depends on specimen related features and spatial resolution required for the measurements.

Table 1
Chemical compositions of AISI P20 tool steel powder and wrought substrate (wt.%).

Element	Powder	Substrate
Chromium	1.86	1.40–2.0
Molybdenum	0.53	0.30–0.55
Manganese	0.83	0.60–1.0
Silicon	0.67	0.20–0.80
Copper	0.02	
Carbon	0.40	0.28–0.4
Sulfur	0.01	
Phosphorus	0.01	
Iron	Remainder	Remainder

This paper presents an experimental study on process-induced residual stresses in laser clad AISI P20 tool steel onto pre-hardened wrought P20 base material (or substrate) and their correlation with microstructure evolution. Since the hole-drilling method (ASTM E837-95) is relatively accessible, only overall values of the residual stresses are provided in the clad; while the neutron diffraction can provide profiles of residual stresses across the clad and substrate, both methods were employed in the current comparative investigation. X-ray diffraction (XRD), scanning electron microscope (SEM) and microhardness tester were used to study the microstructures in the laser clad P20 tool steel. Combined with the above experimental analyses, the roles of solid-state phase transformations in the clad and HAZ of the substrate on the development and controllability of residual stresses in the clad have been discussed, and the results thus obtained could be used to effectively repair damaged plastic injection molds made by P20 tool steel.

2. Experimental

2.1. Cladding and substrate materials

The commercial Micro-Melt® P20 tool steel powder manufactured by Carpenter Powder Products Inc. (Bridgeville, PA) was used as cladding material. The powder was spherical in shape with a size range of 44–63 μm (−230/+325 mesh). Wrought AISI P20 tool steel plate with a thickness of about 10 mm, was used as a substrate for laser cladding. Prior to cladding, the base material was austenitized at 845 °C, and then quenched into the water and subsequently, tempered at 205 °C for 2 h. The surface of the P20 substrate was grounded and degreased with acetone in order to maintain a consistent absorption of laser beam during cladding. The chemical compositions of the P20 tool steel powder and substrate are listed in Table 1.

2.2. Laser cladding process and post-cladding stress-relieving treatments

The laser cladding process with injecting powder feedstock, illustrated in Fig. 1a, was used for the current study. The experimental setup employed a 3 kW continuous wave (CW) CO_2 laser (model: GE Fanuc C3000), a precision powder feeder (model: Mark

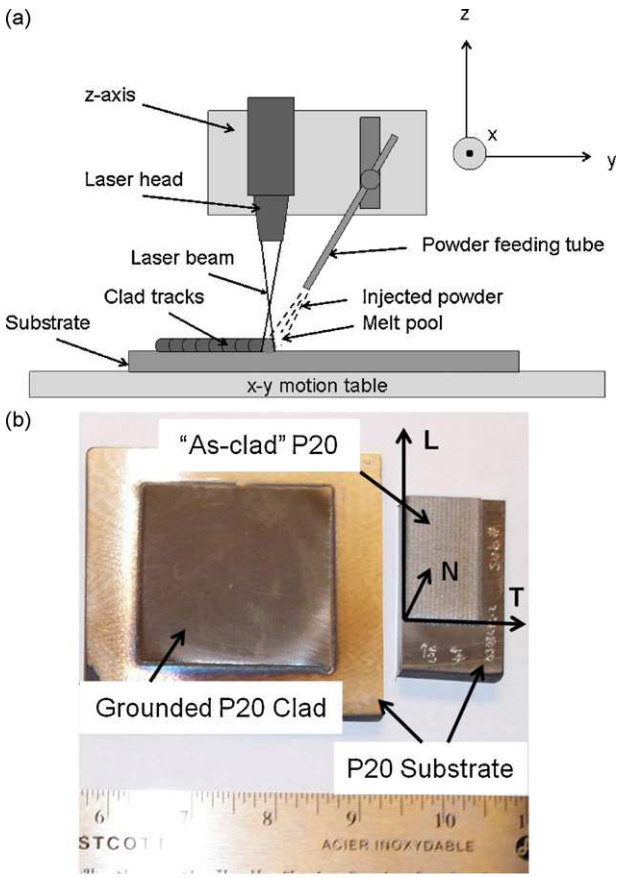

Fig. 1. (a) An illustration of laser cladding process by blowing powder feedstock and (b) laser clad P20 tool steel specimens, where the "L" is referred to the longitudinal direction of laser cladding, and the "T" is designated as the transverse direction of the laser cladding while the "N" is the normal to the surface of the clad.

XV-RC), and a computer numerically controlled (CNC) motion system. Both laser focusing optics and powder feeding nozzle were mounted on the *z*-axis of the CNC motion system while a hardened P20 substrate was clamped on the *x*–*y* motion table. Laser cladding was carried out in a glove box filled with argon to maintain an oxygen level below 50 ppm. In addition, the argon was also used as a carrying gas for the delivery of the P20 powder and a shielding gas for the laser optics during the process.

During laser cladding, a 190 mm focal length lens was used to focus a laser beam onto a substrate to create a melt pool (~3 mm in diameter) along with the melting of injected powder delivered at a feed rate of 10–15 g/min. With a traversing speed of 7–12 mm/s, a track of the molten material was deposited onto the substrate and rapidly solidified to form a clad bead that was metallurgically bonded to the substrate. By re-melting a portion of the preceding clad track and the substrate, along with injected powder, the second clad bead was deposited neighboring to the first one. Repeatedly, the first layer of the clad was formed by multiple partially overlapped clad tracks. Subsequent layers can be further deposited onto the previous layers whereby they were effectively the new substrate. For the current study, the specimens with three clad layers were produced with a total thickness of about 1.5 mm, where the nominal clad coverage used for the neutron diffraction measurement (see the large specimen on the left side of Fig. 1b) is about 50 mm × 50 mm and the one used for the feasibility study of post-cladding heat treatments (see the relative small specimen on the right side of Fig. 1b) is about 18 mm × 50 mm. In order to investigate the role of post-cladding stress-relieving treatments on the laser clad P20 tool steel, tempering was performed on the clad specimens at 204 °C (400 °F), 316 °C (600 °F), 427 °C (800 °F), and 538 °C (1000 °F) for 1 h, respectively.

2.3. Microstructure characterization

After the process, laser clad P20 plates were mechanically cross-sectioned, polished and chemically etched for metallographic study. The morphology of the clad was observed using an Olympus optical microscope (OM) while its microstructure was studied using a Hitachi S-3500 variable pressure scanning electron microscope (VP-SEM) along with an Oxford energy dispersive spectrometer (EDS). The phases presented in the clad were identified using a Philips X'Pert X-ray diffractometer (XRD) with a graphite-monochromatic CuK_α radiation (λ = ~1.54 Å). Two pairs of diffraction peaks $\alpha\{2\,0\,0\}$–$\gamma'\{2\,0\,0\}$ and $\alpha\{2\,1\,1\}$–$\gamma'\{2\,0\,0\}$ were selected for measuring their relative intensities in which the α and γ' represent martensite and retained austenite, respectively, in the clad. Since the quantity of the carbides in the laser clad P20 specimens was low and difficult to be determined, in this case, the amount of the carbide in the clad was neglected, and the volume fractions of the α and γ' phases in the clad could be approximately estimated by their respective X-ray diffraction intensities using conventional "direct comparison" method [30].

The hardness of the clad and substrate were measured using a Rockwell hardness testing system (model: ME-2, NewAge Industries Testing Instruments Division, Willow Grove, PA). Any hardness data reported here were statistic averages of at least five measurements. The microhardness profiles across the clad and substrate were measured on a microhardness tester (model: MicroMET II, Buehler Ltd., Lake Bluff, IL) using a Vickers indentor with 0.2 kg normal load applied for 15 s.

2.4. Residual stress determination

The surfaces of laser clad P20 specimens were grounded prior to hole-drilling and neutron diffraction measurements.

2.4.1. Hole-drilling method (ASTM E837-95)

Hole-drilling strain-gage method as per ASTM E837-95 was used to measure residual stresses in a clad layer. The measurements were conducted by using an RS-200 milling guide and a strain measurement system (model: 5000, Vishay Intertechnology, Inc., Raleigh, NC). A special strain gage rosette (type: TEA-06-062RK-120) was glued on the surface of the clad specimen where the relieved strains were to be measured. A high-speed air turbine mill with a carbide cutter was used to drill a flat-bottom hole at the centre of the rosette, while the relieved strains in the vicinity of the hole were measured by the strain gage rosette. The residual stresses were then deduced using ReStress® software supplied with the system. The stresses thus obtained reflect the local average values in the clad across a depth of about 0.6 mm from the clad surface, even though the actual residual stresses are non-uniform through the thickness of the clad. The modulus used in the deduction of residual stresses in the P20 clad is 210.3 GPa [9].

2.4.2. Neutron diffraction method

Spatially resolved neutron diffraction measurements of strain in laser clad P20 specimens were conducted by using the L3 neutron diffractometer (Fig. 2a) located at National Research Council's Canadian Neutron Beam Centre (NRC-CNBC, Chalk River, ON, Canada). A monochromatic neutron beam with a nominal wavelength (λ) of ~1.54 Å, was obtained from the (1 1 5) reflection of a germanium (Ge) single crystal. For the measurement of "as-clad" P20 specimen, strains were obtained using its martensite {1 1 2} reflection, with a nominal Bragg angle of ~83.9° for this wavelength. The size and shape of the incident and diffracted neutron beams were

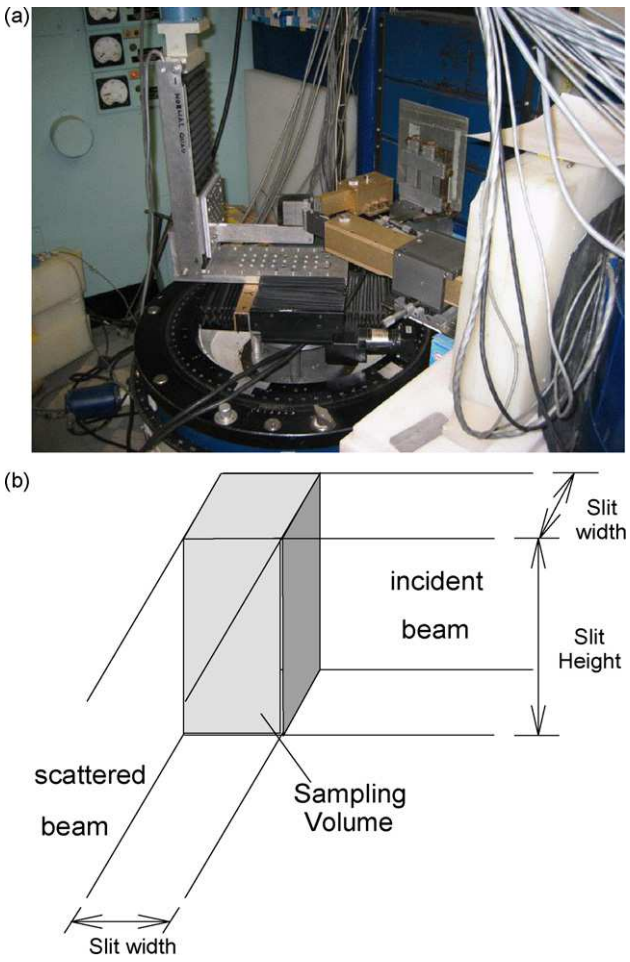

Fig. 2. (a) Neutron diffraction experimental set-up on L3 diffractometer and (b) an illumination of sampling (or scattering) volume.

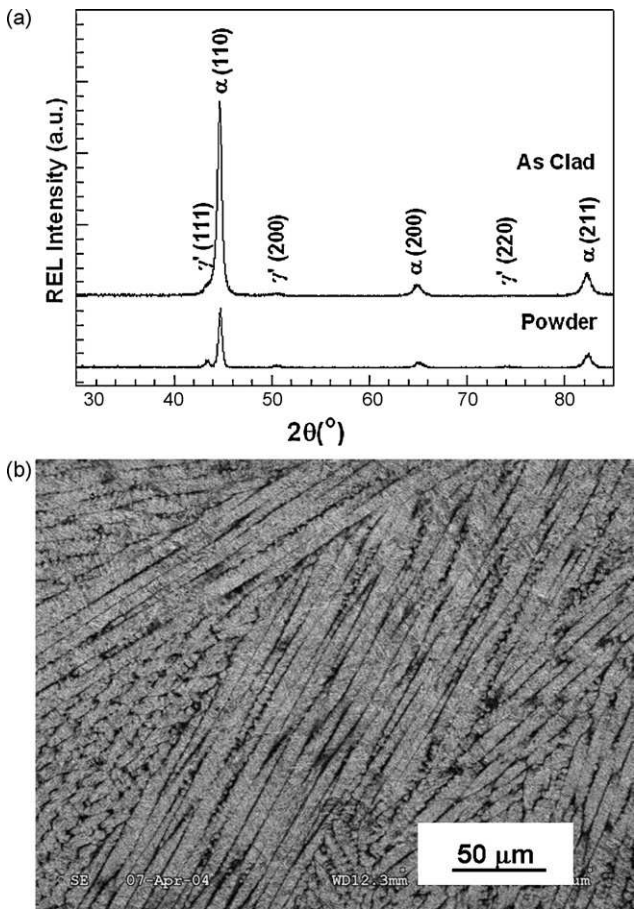

Fig. 3. (a) XRD pattern and (b) SEM microstructure of laser clad P20 specimen in "as-clad" condition.

defined by rectangular slits of finite width (0.3 mm) cut in neutron absorbing cadmium (Cd) on both the incident and scattered flight-paths of the diffractometer, and the intersection of the incident and diffracted beams defined a sampling or scattering volume of 0.3 mm (W) × 0.3 mm (W) × 20 mm (H) (Fig. 2b).

The strain measurements were carried out through the thickness of the clad and substrate in an "as-clad" P20 specimen, such that the scan path of scattering volume coincides with face-centre of the clad specimen. Calculations of the stresses were carried out by using elastic constants $E_{\{112\}} = 223$ GPa, and $\nu_{\{112\}} = 0.27$ that were deduced from the single crystal elastic constants of ferrite [31] using the method of Hauk and Kockelmann [32]. Stresses were obtained from the direction along the laser cladding denoted as L, the direction transverse to the laser cladding denoted as T and the normal to the surface of the clad defined as N (Fig. 1b).

3. Results and discussion

3.1. "As-clad" P20 tool steel

In this section, "as-clad" P20 specimens refer to those used for the neutron diffraction measurements with a nominal clad coverage of about 50 mm (L) × 50 mm (T).

3.1.1. Microstructure and phases

The processing parameters for laser cladding of P20 tool steel have been optimized to produce metallurgically sound and dense clad. No cracking and a few porosities were observed within the clad, but all clad specimens showed slightly bent surface, presenting a concave profile toward the clad surface.

The XRD pattern reveals that "as-clad" P20 specimen contains a large amount of martensite (α) plus a small amount of retained austenite (γ′) (Fig. 3a). For comparison, the XRD pattern of P20 tool steel powder was also included in that figure. Nevertheless, any diffraction peaks associated with the carbides in the P20 clad could not be observed within the current resolution. The relative volume fraction of the retained austenite in the "as-clad" P20 clad is about 9.2 vol.% on average.

Fig. 3b presents SEM micrograph of the cross-sectioned P20 specimen in "as-clad" condition, where its microstructure can be characterized as columnar dendritic structure with different orientations. The statistic average of the primary dendritic arm spacing (DAS) is about 7 μm. The refined microstructure implies that the clad material experienced a relatively rapid solidification during cladding, which could be beneficial to the improvement of resultant mechanical properties of the clad material.

3.1.2. Through-thickness profile of microhardness

Fig. 4a presents a microhardness profile across the thickness of an "as-clad" P20 specimen, where the solid line marks an interface between the clad and the substrate before laser cladding. After cladding, a mixture of the cladding material and substrate created a penetration zone between the solid and dash line. Measured with an optical microscope, the thickness of the clad and the depth of the penetration zone for the P20 clad specimen are about 1.42 and 0.1 mm, respectively. The average microhardness of the clad

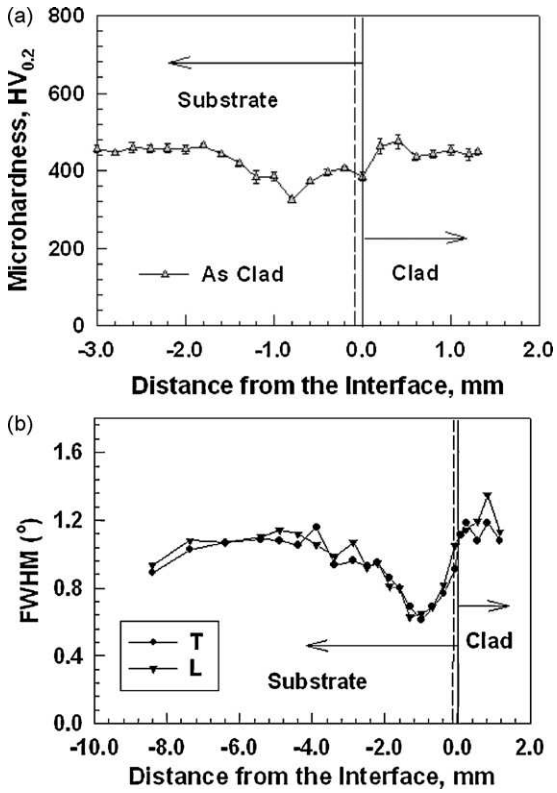

Fig. 4. (a) Through-thickness profile of microhardness and (b) through-thickness variation in diffraction peak width (FWHM) of "as-clad" P20 specimen.

and the bulk substrate have no obvious difference: about 454 and 451 HV, respectively. There is a decrease in the microhardness at the penetration zone and the surrounding heat-affected zone (HAZ) in the substrate (their total width is estimated to be about 2 mm): about 384 HV.

Compared to the original low-tempered martensite (α') in the P20 substrate, the resultant microstructure at the HAZ is medium- or high-tempered martensite due to self-tempering, which has been confirmed in both neutron diffraction measurement and microhardness testing. Fig. 4b illustrates the through-thickness profiles in the variation of diffraction peak width (expressed as the full width at half-maximum height, FWHM) in the "as-clad" P20 specimen. A reduced FWHM was observed in the HAZ nearby the interface. It is understood that the crystal structure of martensite is tetragonal close-packed, the degree of tetragonality (normally characterized by the "c/a" ratio) is directly correlated with carbon concentration within the martensite, and diffraction peaks of the martensite are systematically broader than those observed in ferrite due to overlap between variants of the martensitic crystal lattice reflections (in the present case, {1 1 2}, {1 2 1} and {2 1 1}). Thus, the reduced FWHM implies a loss of tetragonality induced by carbide precipitation in the original low-tempered martensite at the HAZ. Moreover, a larger decrease in the FWHM corresponds to a greater loss of carbon concentration in the original low-tempered martensite, which, in return, indicates that the microstructure has been gradually evolved into medium- or high-tempered martensite. On the other hand, as stated before, the through-thickness profile in the microhardness of the "as-clad" P20 specimen reveals that as compared with the original substrate, the HAZ experienced a reduction in its microhardness, which also indicates the presence of a substantial self-tempering during cladding. Hence, both neutron diffraction and microhardness measurement have reached the same conclusion.

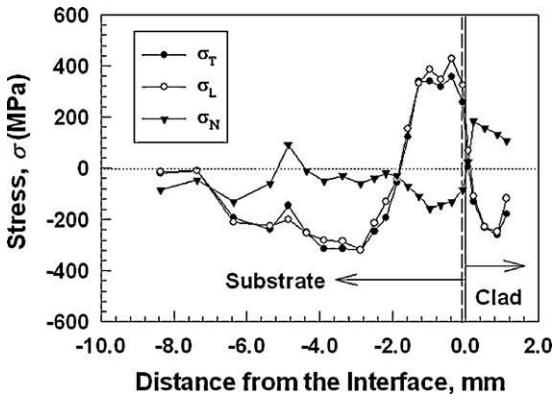

Fig. 5. Through-thickness profiles of residual stresses in "as-clad" P20 specimen.

3.1.3. Through-thickness profiles of residual stresses

Fig. 5 illustrates the through-thickness profiles of residual stresses in an "as-clad" P20 specimen measured by neutron diffraction, in which the σ_L represents the stress in the direction of laser cladding and the σ_T in the direction transverse to the laser cladding while the σ_N normal to the surface of the clad layer. Through examining the stress profiles, three distinct regions can be found within the clad specimen. The first region closest to the surface of the clad with a depth of about 1.4 mm (but still within the clad) indicates the presence of biaxial compressive residual stresses with its maximum value of around 260 MPa at a depth of 0.4–0.6 mm from the surface of the clad. The stress is tensile in the normal direction of the clad specimen. The interface of the second region appears as a sharp stress gradient at a depth of about 1.4 mm from the surface of the clad, where the sign of the in-plane stress switches from the compression to the tension. From the optical examination of the P20 clad specimen, the location of this stress gradient corresponds approximately to the interface between the clad and the substrate marked by the solid line in that figure. Large biaxial tensile stresses are observed within this region with a depth of about 2 mm, while compressive stress exists in the normal direction. Immediately after the second region, which is at a depth of 3–3.5 mm from the clad surface, a third distinct region is observed where the sign of the in-plane stresses switches again from the tension to the compression, and beyond this region the profile varies smoothly from the compression to a state of near zero stresses at the rear surface of the clad specimen. The overall residual stress profiles appear to be reproducible from another P20 clad specimen produced with identical processing parameters. This indicates that the present laser cladding process has a good repeatability.

Comparatively, the residual stresses (σ_L and σ_T) measured through hole-drilling method in the same specimen are -241 ± 29 and -229 ± 62 MPa, respectively. The conventional method confirms that biaxial compression exists in the "as-clad" P20 specimen. It should be noted that in the current case the residual stresses determined through the hole-drilling method only represent average across a depth of about 0.6 mm from the surface of the clad, while the neutron diffraction reveals the depth profiles of residual stresses across the clad and substrate.

3.1.4. Residual stress analysis

The development of residual stresses in a clad during laser cladding is a complex process which not only depends on thermal effects generated by the laser beam but also on temperature-dependent physical and mechanical responses of the materials involved. There are two main origins of residual stresses in the P20 clad. The first source comes from thermal shrinkage in the clad that is constrained by the cold substrate as the clad cools after it re-solidifies, generating tensile residual stresses in the clad. The

second source comes from "austenite-to-martensite" transformations ($\gamma \rightarrow \alpha$ and $\gamma' \rightarrow \alpha'$) occurred in the clad, once again, when the clad cools after it re-solidifies, generating significant amount of volumetric expansion in the clad, which could partially or entirely cancel, or even exceed the thermal-shrinkage-induced volumetric contraction in the clad and consequently, could reduce the magnitude of the tensile residual stresses, or even result in compressive residual stresses in the clad instead.

Regarding effects of phase transformation on volumetric change in a clad, it should be noted that a typical martensitic transformation ($\gamma \rightarrow \alpha$) is usually unable to transform all high-temperature austenite (γ) into martensite (α) and consequently, a certain amount of retained austenite (γ') would remain in the clad at the room temperature after cladding. The presence of the retained austenite which has less specific volume as compared to the martensite, however, adversely affects any efforts to reduce the magnitude of tensile residual stresses induced by thermal shrinkage in the clad. Fortunately, the retained austenite is thermally unstable and could subsequently be transformed into tempered martensite (α') if a tempering is applied in the clad. In reality, some of the retained austenite remained in the "as-clad" P20 layer was indeed transformed into tempered martensite (i.e., $\gamma' \rightarrow \alpha'$) since the clad specimen would be inevitably subjected to repeatedly re-heating during laser cladding process. As described in Section 2.2, during cladding, a portion of previously deposited layer was always re-heated by subsequently deposited layer. If the dimensions of the substrate are not large enough to ensure its effectiveness as a "heat sink", the accumulated heat in the whole clad specimen may eventually induce a "self-tempering" on the clad. For the current "as-clad" P20 specimen used for the neutron diffraction study, the thermal mass of the P20 clad layer accounts for about 6.2% of total mass of the clad specimen. It was, in fact, observed that after cladding the clad plate became very hot. The heat, in varying degree, contributed to the self-tempering in the clad, which produced tempered martensite, partially at the expense of the retained austenite. The experimental results have shown that the overall volumetric expansion induced by the phase transformations ($\gamma \rightarrow \alpha$ and $\gamma' \rightarrow \alpha'$) has changed the sign of the resultant residual stresses in the clad from the tension to the compression.

Heat-affected zone (HAZ) in the substrate may also have significant effects on the distortion and the resultant distribution of residual stresses within a clad specimen. Pilloz et al. [13] studied process-induced residual stresses in laser cladding of nickel-based alloy on low carbon steel XC10; while Dubourg et al. [14] investigated Al50Si alloy cladding on 5052 aluminum substrate. By using a proposed phenomenological model (or block model) [13], both papers concluded that in addition to the clad and unaffected cold bulk substrate, the HAZ plays an important role in the resultant distribution of residual stresses in the clad specimens through thermal shrinkage [14] and/or volumetric change induced by solid-state phase transformations [13] when both clad and HAZ cool, which determines the final distorted shape of the clad specimens. In our case, both clad and substrate is made up by the same P20 material, and their coefficients of thermal expansion (CTEs) are almost identical. In addition, not only the clad but also HAZ experienced a solid-state martensitic transformation when the clad and HAZ cool. Hence, based on the observation on the distortion of the laser clad P20 plate along with our residual stress measurements, we propose the following mechanism to explain effects of the clad and HAZ on the distortion and residual stress distribution in our clad specimen.

During cladding, a melt pool was created, which also heated up a portion of underneath P20 substrate to form a HAZ. At a region of the HAZ directly beneath the melt pool, its prior low-tempered martensite (α') would be re-austenitized to form high-temperature austenite (γ) while the prior low-tempered martensite in a region of the HAZ further away from the melt pool would be tempered in a varying degree, depending on their local temperatures. Thus, as the melt pool solidified to form the clad and continued to cool but prior to its martensitic transformation temperature (M_s), a simultaneous thermal shrinkage in the clad and re-austenitized region of the HAZ would generate global tensile stresses due to the constraint brought by the unaffected cold substrate. On the other hand, the volumetric shrinkage also occurred at the rest of the HAZ due to severe tempering, causing the prior low-tempered martensite to be de-composited into the medium- or high-tempered martensite along with carbide precipitation. This would lead to tensile stresses at that region too. The tensile stresses in the clad and the entire HAZ would be balanced by the compressive stresses in the unaffected cold substrate. As a result, the clad specimen would show a concave shape if the substrate was not thick enough to resist the distortion (see Fig. 6a).

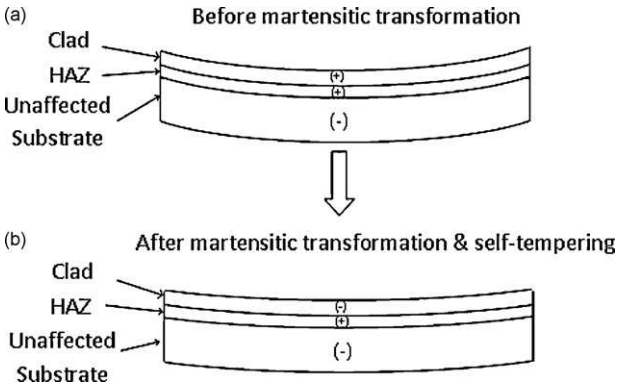

Fig. 6. Schematic presentation of the sign of residual stresses in the P20 clad, heat-affected zone (HAZ), and unaffected substrate.

However, the clad experienced a martensitic transformation ($\gamma \rightarrow \alpha$) to form quenched martensite (α) plus retained austenite (γ') once the clad specimen cooled down to below its M_s and subsequently, the quenched martensite and some of the retained austenite would be de-composited into the low-tempered martensite (i.e., $\alpha \rightarrow \alpha'$ and $\gamma' \rightarrow \alpha'$), when subjected to a repeated self-tempering, expanding its volume. Meanwhile, the re-austenitized region of the HAZ almost simultaneously experienced similar types of phase transformations (i.e., $\gamma \rightarrow \alpha$, and then $\alpha \rightarrow \alpha'$ plus $\gamma' \rightarrow \alpha'$), and also changed its volume within that region. As compared with the original low-tempered martensite in the substrate, the resultant microstructure in the entire HAZ has actually developed into the medium- or high-tempered martensite due to such kind of thermal effects (see the discussion in Section 3.1.2), causing an overall volumetric contraction instead. As a result, the volumetric expansion in the clad, constrained by the contracted HAZ, added certain amount of compression into the existing tension in the clad while the contracted HAZ, restricted by the surrounding clad and unaffected cold substrate, accordingly added more tension into the existing tension in the HAZ. Moreover, the overall martensite-transformation-induced volumetric change in the clad would be much more than that occurred in the HAZ. This finally reversed the sign of the resultant residual stresses in the clad from the tension to the compression while the residual stresses in the HAZ generated much higher tension instead. Furthermore the compressive stresses would still remain in the unaffected bulk substrate due to no presence of any solid-state phase transformation (although minor self-adjustment may occur to balance the stresses within the clad and HAZ). Finally, the magnitude of volumetric expansion in the clad might not be large enough to restore the concave shape back to flat but could reduce certain amount of distortion in the clad specimen (see Fig. 6b).

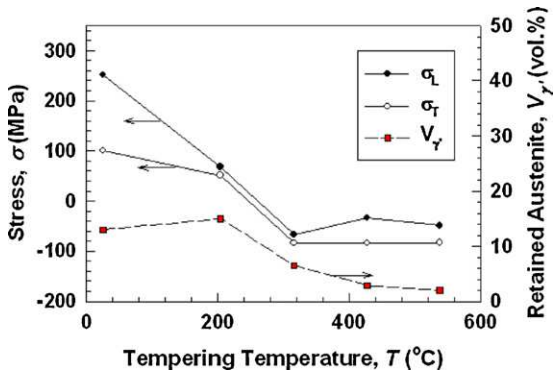

Fig. 7. The amount of residual stresses (σ_L and σ_T) and retained austenite (γ') in the post-cladding heat treated laser clad P20 specimens with less clad coverage *vs.* tempering temperature.

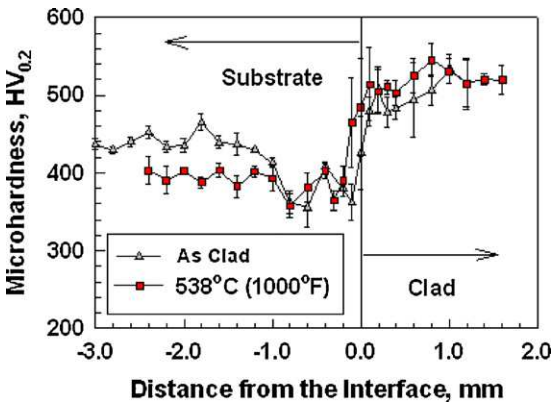

Fig. 8. Through-thickness profiles of microhardness in the post-cladding heat-treated laser clad P20 specimens with less clad coverage.

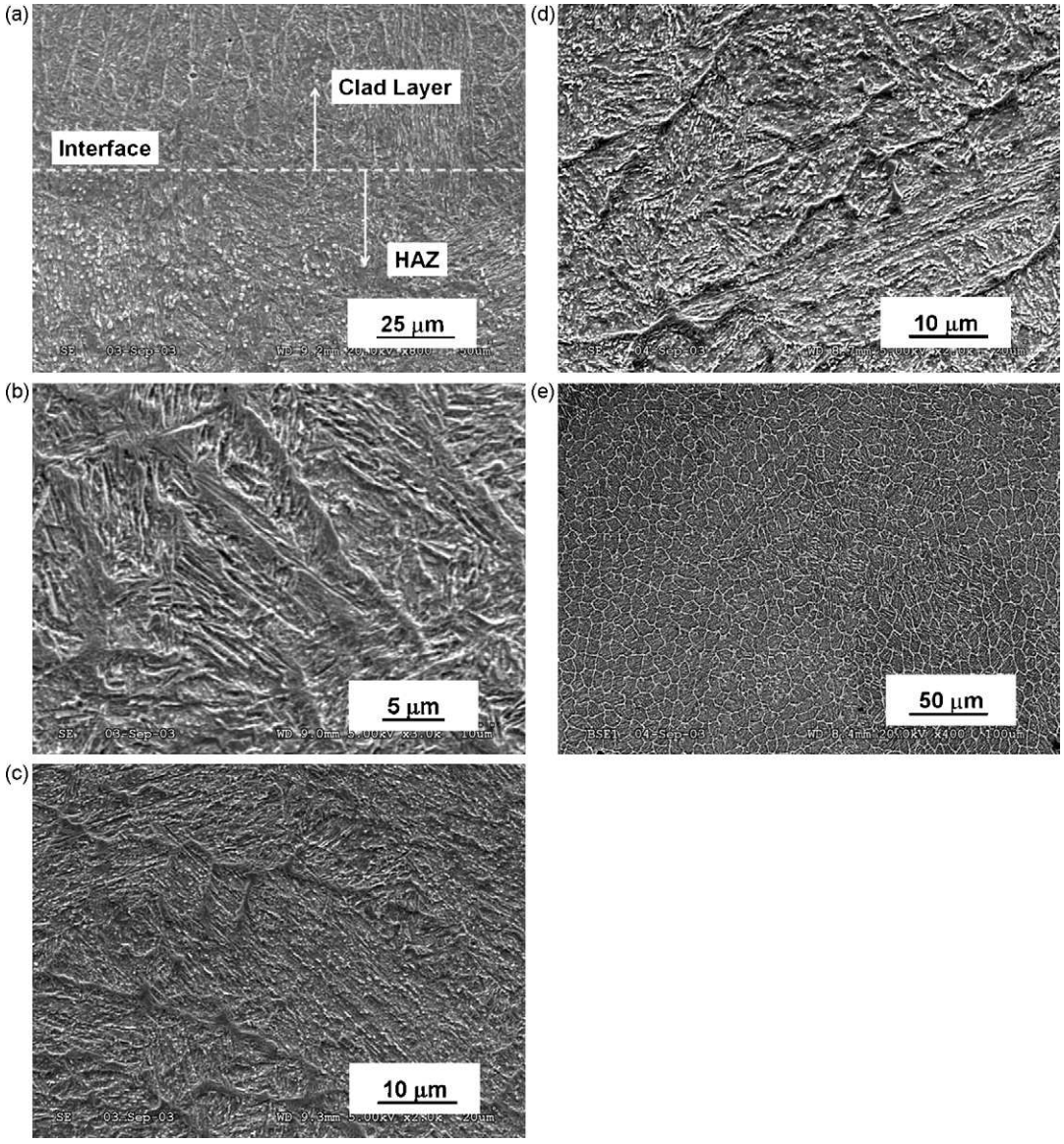

Fig. 9. SEM micrographs of laser clad P20 tool steel with less clad coverage: (a) "as-clad", and tempered at (b) 204 °C, (c) 316 °C and (d), (e) 538 °C for 1 h, respectively.

3.2. "Heat sink" effect and post-cladding stress-relieving treatments

It has been observed that even the same clad material produced with the same processing parameters but different amount of clad coverage and size of substrate could generate different magnitude and sign of residual stresses in "as-clad" specimen. Either tensile or compressive stresses are possible because different process-induced cooling rates could produce quite different amounts of retained austenite (γ'), and different magnitude of self-tempering in the clad and HAZ.

In the following study, the P20 clad specimens with the nominal clad coverage of 18 mm (L) × 50 mm (W) were used to investigate effects of post-cladding stress-relieving treatments on residual stresses in the clad. The clad coverage of these specimens accounts for almost 36% of the total clad coverage of those used for the neutron diffraction investigation. Consequently, the resultant microstructure and microhardness in both "as-clad" P20 specimens show noticeable differences. For a relative volume fraction of the retained austenite (γ') in the clad: the former contains about 13 vol.%, which results in tensile residual stresses in the clad (see Fig. 7); while the latter contains about 9.2 vol.%, which, in return, generates compressive residual stresses in the clad (see Fig. 5). For the microhardness in the clad, the former is about 500 HV; while the latter is about 454 HV. Both HAZs in the substrate show similar low microhardness (~380 HV) due to severe self-tempering effect. These findings implicate that the substrate has "heat sink" effect, and its effectiveness could particularly affect the resultant residual stresses in the clad plates.

A series of post-cladding stress-relieving treatments (or tempering) have been conducted on the above specimens with less amount of clad coverage. In Fig. 8, prior to any tempering, the average microhardness in the "as-clad" layer, HAZ and unaffected substrate are about 500, 380, and 440 HV, respectively. Immediately after tempered at 538 °C, the microhardness difference between the HAZ and the unaffected substrate completely disappears, and both reach about 396 HV while the average microhardness in the heat-treated clad has slightly increased to about 521 HV instead. This increase in the microhardness of the clad might be ascribed to the fine carbide precipitation since the microhardness is less correlated with the amount of retained austenite (γ') in the clad. For instance, when tempered at 316 °C, most of retained austenite in the clad has already been transformed into tempered martensite (α'), however, its hardness remained almost unchanged. Moreover, it is also noted that the HAZ in the "as-clad" P20 specimen experienced an equivalent high-temperature tempering during cladding since its microhardness was almost as the same as that of the substrate subjected to a tempering at 538 °C.

For the current specimens with less amount of clad coverage, the SEM observation of the "as-clad" P20 and HAZ reveals that the clad exhibits refined dendrites while the HAZ in the substrate shows the presence of a large amount of carbide precipitates that again implies an occurrence of a severe self-tempering (Fig. 9a). Tempered at 206 °C, the quenched martensite (α) in the clad was still stable and the carbide precipitation in the martensitic matrix can barely be seen (Fig. 9b). After tempered at a temperature from 316 to 538 °C, the quenched martensite in the clad was progressively transformed into medium- or high-tempered martensite (α') and fine carbides were gradually precipitated between the martensitic lathes (Fig. 9c and d) but still retained the characteristics of the columnar dendritic structure in the clad (Fig. 9e).

It is noted that the amount of retained austenite (γ') and carbide precipitates significantly affect the sign and magnitude of the resultant residual stresses in the P20 clad. Tempering has successfully reduced the amount of retained austenite and induced carbide precipitation and as a result, for the P20 specimens with less amount of clad coverage, the magnitude and the sign of residual stresses in the clad were changed (Fig. 7). When the relative volume fraction of retained austenite in the clad is 13–15 vol.%, the resultant residual stresses in the clad show biaxial tensile stresses. When tempered at a temperature from 316 to 538 °C, the relative volume fraction of retained austenite in the clad was significantly reduced and the resultant residual stresses in the clad changed to biaxial compressive stresses instead. For example, when tempered at 538 °C for 1 h, the relative volume fraction of retained austenite in the clad is less than 2 vol.%, and the resultant residual stresses (σ_L and σ_T) in the clad determined by the hole-drilling method are about −49 and −83 MPa, respectively.

4. Concluding remarks

Using laser cladding, crack-free and metallurgically sound AISI P20 tool steel clad has been produced without pre-heating. The preliminary experimental investigation on profiles of process-induced residual stresses across the thickness of the clad specimens has been carried out using neutron diffraction in combined with hole-drilling method, microhardness measurement and microstructure analysis. Based on the studies, the following conclusions could be made:

- The microstructure in "as-clad" P20 material shows refined columnar dendritic structure that contains a large amount of martensite plus a small amount of retained austenite.
- The through-thickness profiles of residual stresses in the "as-clad" P20 specimen with large clad coverage have been measured. The clad shows biaxial compressive stresses while the heat-affected zone (HAZ) in the substrate reveals biaxial tensile stresses, and the rest of unaffected bulk substrate displays biaxial compressive stresses.
- The amount of clad coverage and the size of substrate affect the magnitude and sign of resultant residual stresses across the thickness of P20 clad specimens since the "as-clad" P20 specimens produced by the same laser processing parameters but with less amount of clad coverage onto the substrate, have showed tensile instead of compressive stresses in the clad.
- Post-cladding stress-relieving treatments (i.e., tempering) could significantly influence the magnitude and sign of resultant residual stresses in the clad, which is correlated with the changes in the volume fraction of retained austenite in the clad.

Acknowledgements

Authors would like to thank J. Fenner, Technical Officer of NRC-IMI-London, for the process development of laser clad P20 tool steel. Canadian Institute for Neutron Scattering (CINS) program sponsored the neutron diffraction measurements in this research. Authors also would like to acknowledge Dr. S. Nikumb, Group Leader of Laser and Materials Processing of NRC-IMI-London for his review and comments on the paper.

References

[1] W.M. Steen, Laser Material Processing, 2nd ed., Springer, London, UK, 1998, pp. 248–251.
[2] E. Toyserkani, A. Khajepour, S. Corbin, Laser Cladding, CRC Press, Boca Raton, FL, USA, 2005, pp. 3–18.
[3] J. Archambeault, L. Dubourg, ICALEO 2005, October 31–November 3, Laser Institute of America, Miami, FL, USA, 2005, pp. 570–579.
[4] L. Xue, J.-Y. Chen, C.V. Hyatt, M.U. Islam, Proceedings of 8th CF/CRAD Meeting on Naval Applications of Materials Technology, May 11–13, Halifax, NS, Canada, 1999, pp. 288–302.
[5] L. Xue, J.-Y. Chen, G. Campbell, S.-H. Wang, Invited Presentation for MMO Workshop on Automated and Intelligent Systems for High Performance Mold Finishing Processes, November 27, 2003, Toronto, ON, Canada, 2003.

[6] L. Xue, J.-Y. Chen, S.-H. Wang, Y. Li, Symposium on Processing & Product Manufacturing: Joining of Advanced & Specialty Materials IX: Repair & Manufacture of Industrial Gas Turbines & Aero-Engine Components in Materials Science & Technology 2007 (MS&T'07), September 16–20, ASM International, Detroit, MI, 2007, pp. 315–328.
[7] J.-Y. Chen, L. Xue, H. Visscher, J. Wolfe, Symposium on Surface Protection for Enhanced Material Performance in Materials Science & Technology 2009 (MS&T'09), October 25–29, ASM International, Pittsburgh, PA, USA, 2009, pp. 2090–2101.
[8] J.-Y. Chen, L. Xue, Symposium on Processing and Product Manufacturing: High Performance Tooling Materials in Materials Science & Technology 2010 (MS&T'10), October 17–21, ASM International, Houston, TX, USA, 2010.
[9] Engineering Alloys Digest Inc., AISI Type P20, Alloy Digest, January 1982.
[10] W.T. Preciado, C.E.N. Bohorquez, J. Mater. Process. Technol. 179 (2006) 244–250.
[11] J.-Y. Chen, L. Xue, in: O. Popoola, N.B. Dahotre, J.O. Iroh, D.H. Herring, S. Midea, H. Kopech (Eds.), Proc. 1st ASM International Surface Engineering and 13th IFHTSE Congress, October 7–10, Columbus, OH, USA, 2002, pp. 198–205.
[12] J. Tuominen, P. Vuoristo, T. Mantyla, ICALEO 2005, October 31–November 3, Laser Institute of America, Miami, FL, USA, 2005, pp. 635–639.
[13] M. Pilloz, J.M. Pelletier, A.B. Vannes, J. Mater. Sci. 27 (1992) 1240–1244.
[14] L. Dubourg, F. Hlawka, A. Cornet, in: T.S. Sudarshan, M. Jeandin, J.J. Stiglich (Eds.), Surface Modification Technologies XVIII, ASM International, Materials Park, OH, USA, 2006, pp. 331–334.
[15] J.-Y. Chen, S.-H. Wang, L. Xue, "A comprehensive investigation on the development and controllability of laser-cladding induced residual stresses", to be submitted to journal for publication, 2010.
[16] R. Dekumbis, Proc. 6th Conf. Lasers in Manufacturing, 10–11 May, IFS Ltd, Birmingham, UK, 1989, pp. 185–192.
[17] J.-Y. Chen, L. Xue, S.-H. Wang, The 5th International Workshop on Advanced Manufacturing Technologies (AMT 2005), May 16–18, London, ON, Canada, 2005, pp. 281–286.
[18] A. Rosselet, in: M. Cross, J. Campbell (Eds.), Modelling of Casting, Welding & Advanced Solidification Processes VII, TMS, 1995, pp. 327–334.
[19] S. Ghosh, J. Choi, J. Laser Appl. 17 (3) (2005) 144–158.
[20] A.M. Deus, J. Mazumder, ICALEO 2006, October 30–November 2, Laser Institute of America, Scottsdale, AZ, USA, 2006, pp. 496–505.
[21] J.M. Sprauel, E. Pluyette, The 9th International Symposium on Progress in Metals & New Materials, November 17, 1993, pp. 21.1–21.10.
[22] E. Pluyette, J.M. Sprauel, Proc. 4th International Conf. On Residual Stresses, June 8–10, Baltimore, Maryland, USA, 1994, pp. 860–869.
[23] J. Grum, M. Znidarsic, Mater. Sci. Forum (Switzerland) 404–407 (2002) 437–444.
[24] J. Grum, M. Znidarsic, Mater. Sci. Forum (Switzerland) 426–432 (2003) 2521–2526.
[25] Y.Y. Santana, J.G. La Barbera-Sosa, M.H. Staia, J. Lesage, E.S. Puchi-Cabrera, D. Chicot, E. Bemporad, Surf. Coatings Technol. 201 (2006) 2092–2098.
[26] P. Bendeich, N. Alam, M. Brandt, D. Carr, K. Short, R. Blevins, C. Curfs, O. Kirstein, G. Atkinson, T. Holden, R. Rogge, Mater. Sci. Eng. A 437 (2006) 70–74.
[27] M.R. James, J. Lu, in: J. Lu (Ed.), Handbook of Measurement of Residual Stresses, Fairmont Press, Lilbum, GA, 1995, p. 4.
[28] J. Lu, M.R. James, L. Mordfin, in: J. Lu (Ed.), Handbook of Measurement of Residual Stresses, Fairmont Press, Lilbum, GA, 1995, pp. 225–232.
[29] U. De Oliveira, V. Ocelik, J.Th.M. De Hosson, Surf. Coatings Technol. 201 (2006) 533–542.
[30] B.D. Cullity, Elements of X-ray Diffraction, Addison-Wesley Publishing Co., Inc., London, UK, 1956, p. 391.
[31] A. Kelly, G.W. Groves, Crytsallography & Crystal Defects, Longman, London, UK, 1970, p. 163.
[32] V. Hauk, H. Kockelmann, Z. Metallkd. 70 (1979) 500–502.